

THE DEEPEST X-RAY LOOK AT THE UNIVERSE

S. CAMPANA¹, A. MORETTI¹, D. LAZZATI², G. TAGLIAFERRI¹*Accepted for publication in ApJ Letters*

ABSTRACT

The origin of the X-ray background, in particular at hard (2–10 keV) energies, has been a debated issue for more than 30 years. The Chandra deep fields provide the deepest look at the X-ray sky and are the best dataset to study the X-ray background. We searched the Chandra Deep Field South for X-ray sources with the aid of a dedicated wavelet-based algorithm. We are able to reconstruct the Log N–Log S source distribution in the soft (0.5–2 keV) and hard (2–10 keV) bands down to limiting fluxes of 2×10^{-17} erg s⁻¹ cm⁻² and 2×10^{-16} erg s⁻¹ cm⁻², respectively. These are a factor ~ 5 deeper than previous investigations. We find that the soft relation continues along the extrapolation from higher fluxes, almost completely accounting for the soft X-ray background. On the contrary, the hard distribution shows a flattening below $\sim 2 \times 10^{-14}$ erg s⁻¹ cm⁻². Nevertheless, we can account for $\gtrsim 68\%$ of the hard X-ray background, with the main uncertainty being the sky flux itself.

Subject headings: diffuse radiation – surveys – cosmology: observations – X-rays: general

1. INTRODUCTION

In the soft (1–2 keV) band, ROSAT surveys resolved 70 – 80% of the cosmic X-Ray Background (XRB) into discrete sources, at a flux level of 1×10^{-15} erg s⁻¹ cm⁻² (Hasinger et al. 1998). The great majority of sources brighter than 5×10^{-15} erg s⁻¹ cm⁻² were optically identified with unobscured Active Galactic Nuclei (AGN; Schmidt et al. 1998; Lehmann et al. 2001). The origin of the background at higher energies is more controversial. The ASCA and *BeppoSAX* deep surveys achieved relatively shallow detection limits of $(3 – 5) \times 10^{-14}$ erg s⁻¹ cm⁻², resolving $\sim 25\%$ of the XRB into point sources (Ogasaka et al. 1998; Cagnoni et al. 1998; della Ceca et al. 2000; Giommi et al. 2000). Main contributors are thought to be absorbed and unabsorbed AGN with a mixture of quasars and narrow emission-line galaxies as optical counterparts (e.g. Fiore et al. 1999; Akiyama et al. 2000). Recently, Chandra and XMM-Newton have dedicated long exposures to address this issue (Mushotzky et al. 2000; Giacconi et al. 2001a; Hornschemeier et al. 2000, 2001; Brandt et al. 2001; Hasinger et al. 2001; Tozzi et al. 2001). The analysis of the first 300 ks of the Chandra Deep Field South (CDFS) allowed to reach limiting fluxes of $\sim 10^{-16}$ erg s⁻¹ cm⁻² (0.5–2 keV) and $\sim 10^{-15}$ erg s⁻¹ cm⁻² (2–10 keV; Tozzi et al. 2001). Similar results were obtained on the Hubble Deep Field by Chandra observations (Hornschemeier et al. 2000, 2001). These observations allowed the resolution of 81 – 95% of the soft (1–2 keV) XRB, confirming the results from the deep ROSAT HRI surveys in the Lockman hole (Hasinger et al. 1998). In the hard band, the absolute value of the background is poorly established and, depending on the adopted normalization, Tozzi et al. (2001) were able to account for 60 – 90% of the hard (2–10 keV) XRB.

The increasing angular resolution and source crowding provided by the current generation of X-ray instruments demands advanced detection algorithms. One of these is the wavelet transform (WT), a mathematical tool for multi-scale image analysis. The automatic detection and characterization of sources in X-ray images by means of WT-based algorithms were first carried out by Rosati et al. (1994, 1995). WT-

based techniques have been developed and applied also by other groups to the analysis of ROSAT images (e.g. Slezak et al. 1994; Grebenev et al. 1995; Damiani et al. 1997; Vikhlinin et al. 1998; Lazzati et al. 1999). In view of the excellent results so far obtained, it is natural to extend these techniques to the analysis of the far richer Chandra images (Freeman et al. 2001; Harnden et al. 2001; Moretti et al. 2001). Here we analyzed the full (0.97 Ms) CDFS (Giacconi et al. 2001b; Rosati et al. 2001) by means of an advanced detection algorithm originally developed for the analysis of the ROSAT HRI fields (Lazzati et al. 1999; Campana et al. 1999) based on the WT (Brera Multiscale Wavelet - BMW). At variance with other WT algorithm, our BMW characterizes detected sources by means of a decimation scheme (Lazzati et al. 1999). The application and testing of this algorithm on Chandra fields and on the CDFS in particular is extensively described in Moretti et al. (2001).

2. CHANDRA OBSERVATIONS

The CDFS consists of eleven observations for a total exposure time of 0.97 Ms. All exposures were taken with the Chandra X-ray Observatory (Weisskopf et al. 2000) Advanced CCD Imaging Spectrometer (ACIS-I) detector (Garmire et al. 2001). ACIS-I consists of four CCDs arranged in a 2×2 array for a field of view of $16.9' \times 16.9'$. The on-axis image quality is $\sim 0.5''$ FWHM, increasing to $\sim 3.0''$ FWHM at $\sim 4.0'$ off-axis. The data were filtered to include only the standard event grades 0, 2, 3, 4 and 6 (see Chandra proposers' observatory guide). All hot pixels and bad columns were removed. We removed also flickering pixels with more than two events contiguous in time (time interval of 3.3 s) and residual cosmic ray events.

The eleven observations were co-added with a pattern recognition routine to within $0.5''$ r.m.s. pointing accuracy (Moretti et al. 2001). We restricted our analysis to the ACIS-I area fully exposed in the eleven observations, selecting a circle with $8'$ radius, for a total coverage of ~ 0.056 deg². In order to compare our results with previous studies we carried out the detection in two selected energy bands: a 0.5–2 keV soft band and a 2–7 keV hard band (in the range 7–10 keV the effective area

¹Osservatorio Astronomico di Brera, Via E. Bianchi 46, Merate (LC), 23807, Italy.²Institute of Astronomy, University of Cambridge, Madingley Road, Cambridge CB3 0HA, UK.

steeply decreases while the background increases resulting in a lower signal to noise ratio for X-ray sources; fluxes in the hard 2–7 keV band are extrapolated to the classical 2–10 keV energy band). Time intervals during which the background rate is larger than 3σ over the quiescent level were removed in each band separately. This results in a net exposure time of 942 ks in the soft band and 936 ks in the hard band. The average background over the fully exposed portion is 0.14 (0.19) counts per square arcsec in the soft (hard) band. Following Tozzi et al. (2001), the count-rate to flux conversion factors in the 0.5–2 keV and in the 2–10 keV bands were computed using the response matrices at the aimpoint. A count rate of 1 count s^{-1} in the soft band corresponds to a flux of $(4.6 \pm 0.1) \times 10^{-12}$ erg s^{-1} cm^{-2} and of $(2.9 \pm 0.3) \times 10^{-11}$ erg s^{-1} cm^{-2} in the hard band. These numbers were computed assuming a Galactic absorbing column of 8×10^{19} cm^{-2} and a power law spectrum with a photon index $\Gamma = 1.4$ (i.e. the slope of the hard XRB). The quoted uncertainties are for photon indices in the range $\Gamma = 1.1 - 1.7$. As shown by Tozzi et al. (2001) a conversion factor changing with flux, in order to follow the hardening of the sources, results in a small variation of the Log N–Log S distribution, at a level of $\sim 5\%$.

A critical parameter in the search of faint sources is represented by the detection threshold. In the context of detection by wavelet algorithms this is usually fixed in terms of spurious sources per field (Lazzati et al. 1998). To compare our results with those reported by Tozzi et al. (2001), we require to have less than 4.3 spurious sources within the selected area (i.e. 6 spurious sources per Chandra field). This threshold has been accurately tested with simulations and the number of spurious sources is well under control (Moretti et al. 2001). This threshold corresponds to a source significance larger than 4σ .

3. LOG N–LOG S RELATIONS IN THE SOFT AND HARD BANDS

We searched the inner image with the BMW-Chandra detection algorithm described in Moretti et al. (2001). We detect 239 and 147 sources in the soft and hard band, respectively. There are 22 sources ($\sim 8\%$ of the total number of detected sources) that are revealed only in the hard band, and 116 sources ($\sim 44\%$) that are revealed only in the soft band.

The sky coverage at a given flux, i.e. the area over which a given source can be detected above our threshold (as due to the varying vignetting, angular resolution and exposure time), has been derived by extensive simulations (100 fields per band) in 4 circular annuli (see Moretti et al. 2001). The inhomogeneities of the ACIS-I field of view, such as gaps between the CCDs, are dealt with thorough simulations.

The flux distribution of the detected sources suffers from the well known Eddington bias (e.g. Hasinger et al. 1993). Faint sources can be detected only if superposed on positive background fluctuations (due either to a faint contaminating source or a statistical background fluctuation) and therefore their fluxes are systematically overestimated by factor as large as 2–3. This bias starts affecting the data at a level of ~ 20 counts in the soft band ($\sim 10^{-16}$ erg s^{-1} cm^{-2}) and ~ 30 counts in the hard band ($\sim 10^{-15}$ erg s^{-1} cm^{-2}). This effect has a stronger impact on the 2–10 keV Log N–Log S, due to the higher value of the background. Following the approach by Vikhlinin et al. (1995), we statistically correct for this bias. The completeness of the detection is then accounted for by the completeness function. The accuracy of the procedure is assured by extensive simulations (see Moretti et al. 2001 and Figs. 4–5 therein).

Our simulations show that we are able to recover the number

source distribution down to 4 corrected counts (11 before the bias correction) in the inner core of the image, declining to 8 corrected counts (14 before correction) in the outskirts for the soft band. For the hard band the limit on the corrected counts are 5 in the center and 10 in the outskirts. These counts give a flux limit in the inner region of 2×10^{-17} erg s^{-1} cm^{-2} in the soft band and 2×10^{-16} erg s^{-1} cm^{-2} in the hard band.

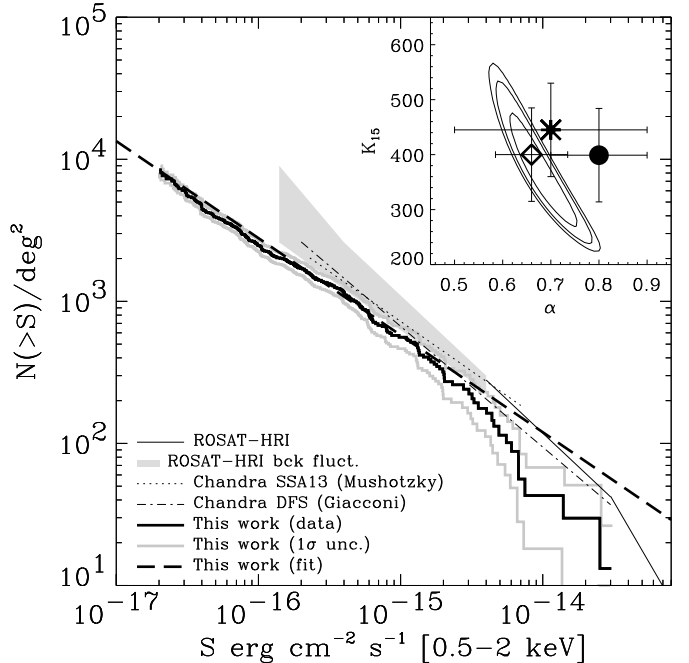


FIG. 1.— Soft band Log N–Log S from inner $8'$ radius of the 1 Ms observation of the CDFS (thick solid line) in the range $2 \times 10^{-17} - 3 \times 10^{-14}$ erg cm^{-2} s^{-1} for an average $\Gamma = 1.4$ power-law spectrum. The gray thick line shows the 1σ confidence region taking into account the number statistics and the flux conversion uncertainties. The thick dashed solid line shows the best M–L fit power law, while the other lines show fits from previous works. The thin solid line shows the ROSAT–HRI results on the Lockman hole (Hasinger et al. 1998); the shaded area shows the result of the background fluctuation analysis of ROSAT–HRI data (Hasinger et al. 1993), while the dotted and dash-dotted lines show the best fit from the analysis of the SSA13 field Mushotzky et al. (2000) and of the first 120 ks on the CDFS Giacconi et al. (2001), respectively. The results on the first 300 ks of the CDFS (Tozzi et al. 2001) are not shown, since they would have been virtually indistinguishable from our best fit line. The inset shows the 1, 2 and 3σ contours from the simultaneous M–L fit of the slope and normalization of the Log N–Log S. The asterisk, circle and diamond are the results of Mushotzky et al. (2000), Giacconi et al. (2001) and Tozzi et al. (2001), respectively.

To characterize the flux distribution of sources detected in the soft band we performed a maximum likelihood fit to the differential (unbinned) source flux distribution with a power-law. We obtain as a best fit:

$$N(>S) = 360 \left(\frac{S}{2 \times 10^{-15}} \right)^{-0.68} \text{ cgs.} \quad (1)$$

Fitting the same data, adaptively binning to 10 sources per bin, we obtain a good fit by means of a χ^2 test (null hypothesis probability $\sim 10\%$). This assures us of the goodness of the fit. The error at 90% confidence level for the normalization is $K_{15} = 360_{-37}^{+41}$ (K_{15} means that fluxes are measured in units of 2×10^{-15} erg s^{-1} cm^{-2}), while the best fit value for the slope is $\alpha_s = -0.68 \pm 0.03$ (see also Fig. 1). Both our normalization and slope, are in good agreement with ROSAT (Hasinger et al. 1998) Chandra (Tozzi et al. 2001, Rosati et al. 2001) and

XMM-Newton (Hasinger et al. 2001) up to their faintest flux levels.

Due to Galactic contributions and following all previous studies, we consider the soft XRB in the 1–2 keV band only. Our fitted Log N–Log S distribution gives an integrated flux of $\sim 5.4 \times 10^{-13}$ erg s $^{-1}$ cm $^{-2}$ deg $^{-2}$ for fluxes fainter than 10^{-15} erg s $^{-1}$ cm $^{-2}$. Summing the contribution at higher fluxes (Hasinger et al. 1998), the total flux of resolved point sources is $\sim 3.5 \times 10^{-12}$ erg s $^{-1}$ cm $^{-2}$ deg $^{-2}$. This accounts for 80% of the unresolved extragalactic background measured by ROSAT and by a joined ASCA/ROSAT analysis (Chen et al. 1997). Extending to even lower fluxes the Log N–Log S distribution (assuming the same slope) we can make up to 85% of the soft XRB, at the most. This is in line with recent predictions for the soft XRB produced by the warm/hot diffuse intergalactic medium which may contribute at a 5–15% level (Phillips et al. 2001). If, instead, we assume the lower (by a factor ~ 0.85) value measured by ASCA (Gendreau et al. 1995), then we are able to account for 96% of the flux in the soft XRB and fully account for it extending the source distribution at the lowest level.

For the hard band our faint limit can be confidently taken down to 2×10^{-16} erg s $^{-1}$ cm $^{-2}$ (see Fig. 2). In order to be consistent with the results at larger fluxes, we normalized our distribution to the ASCA data (della Ceca et al. 2000)³. The Log N–Log S distribution cannot be described with a single power-law (probability of the null hypothesis $\sim 0.02\%$, Fig. 2). We tried to model the data with a broken power-law and with a smoothly-jointed broken power-law. The second function gives a much better agreement with the data and it has the form:

$$N(>S) = 1.2 \times 10^4 \left[\frac{(2 \times 10^{-15})^{\alpha_{h1}}}{S_0^{\alpha_{h1}} + S_0^{\alpha_{h1}-\alpha_{h2}} S^{\alpha_{h2}}} \right] \text{cgs.} \quad (2)$$

To match the bright flux end, we fixed the first slope to the ASCA value, i.e. $\alpha_{h1} = 1.67$ (della Ceca et al. 2000). The maximum likelihood fit yields a faint-end slope $\alpha_{h2} = 0.58 \pm 0.03$ and a break flux $S_0 = 1.7^{+0.3}_{-0.2} \times 10^{-14}$ erg s $^{-1}$ cm $^{-2}$ (all at 90% confidence level for a single parameter; see Fig. 2).

The total contribution to the XRB is then 1.6×10^{-11} erg s $^{-1}$ cm $^{-2}$ deg $^{-2}$. This value has to be compared with the total (unresolved) XRB of 1.6×10^{-11} erg s $^{-1}$ cm $^{-2}$ deg $^{-2}$ from UHURU and HEAO-1 (Marshall et al. 1980), as well as with the more recent determinations from the *BeppoSAX* and ASCA of 2.4×10^{-11} erg s $^{-1}$ cm $^{-2}$ deg $^{-2}$ (Chiappetti et al. 1998; Vecchi et al. 1999; Ueda et al. 1999; Ishisaki et al. 2000; Perri & Giommi 2000), in agreement with the old Wisconsin measurements (McCammon et al. 1983). Our results are in good agreement with the UHURU/HEAO-1 value (considering also the error in the flux determination due to the uncertainties in the background slope, which amounts to 10%). The slope of the faint end counts converges slower than logarithmically and thus the faint sources provide a small contribution to the X-ray background (adding only 10% more extrapolating down to zero flux). In this case we can claim to have fully resolved the 2–10 keV hard XRB. On the contrary, if we adopt the *BeppoSAX* and ASCA value, the fraction of resolved sources in the CDFS lowers to 68%. If we extrapolate our best fit distribution to lower fluxes, we can make up 73% of the entire XRB, at most. If this

were the case a contribution from truly diffuse emission or from a new class of sources has to be advocated.

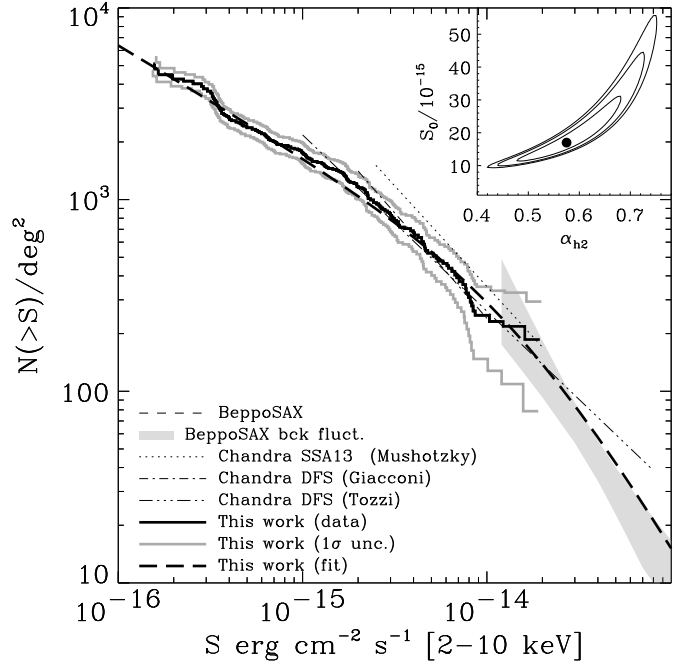


FIG. 2.— Hard band Log N–Log S from inner 8' radius of the 1 Ms observation of the CDFS (thick solid line) in the range $2 \times 10^{-16} - 2 \times 10^{-14}$ erg cm $^{-2}$ s $^{-1}$ for an average $\Gamma = 1.4$ power-law spectrum. The distribution is normalized to the ASCA value and slope (della Ceca et al. 2000). The gray thick line shows the 1σ confidence region taking into account the number statistics and the flux conversion uncertainties. The thick dashed solid line shows the best M–L fit smoothly joined broken power law, while the other lines shows fits from previous works. The thin dashed line shows the *BeppoSAX* result (Vecchi et al. 1999) while the shaded area shows the result of the background fluctuation analysis of *BeppoSAX* data (Perri & Giommi 2000). Lines related to Chandra fields are as in Fig. 1. The inset shows the 1, 2 and 3 σ contours from the simultaneous M–L fit of the faint slope α_{h2} and break flux S_0 , holding the bright slope fixed to the ASCA result and the normalization fixed to the best-fit value (see text).

4. CONCLUSIONS

The origin of the XRB has been extensively studied since its discovery (Giacconi et al. 1962). In the case of the soft (1–2 keV) XRB there is general consensus that the bulk of the emission can be ascribed to broad line AGN (i.e. Seyfert 1 galaxies; Hasinger et al. 1998; Schmidt et al. 1998). At faint fluxes ($\lesssim 10^{-15}$ erg s $^{-1}$ cm $^{-2}$) nearby ($z \lesssim 0.6$) optically-normal galaxies are also being detected as soft sources (Barger et al. 2001; Tozzi et al. 2001; Brandt et al. 2001; Schreier et al. 2001). Our analysis of the CDFS extends these studies down to 2×10^{-17} erg s $^{-1}$ cm $^{-2}$. We found that even at these low fluxes the Log N–Log S distribution can still be represented by the extrapolation from higher fluxes (Tozzi et al. 2001) and we are able to resolve in point sources > 80% of the soft XRB, the main uncertainties being the sky flux itself.

In the hard band the XRB is made by the superposition of absorbed and unabsorbed sources (Setti & Woltjer 1989). In particular, the flat spectrum of the background ($\Gamma \sim 1.4$) implies a considerable absorption in most objects. Several studies have emphasized the importance of the hard XRB as a probe

³This normalization of the Log N–Log S distribution allows to get rid of cosmic variance at bright fluxes. At faint fluxes this is not true and the small field analyzed can play likely a role, e.g. in the Chandra observation of the HDF more sources are detected at the same flux level (Brandt et al. 2001).

of the evolution of the black hole population (Fabian & Iwasawa 1999). The small number of hard sources not detected in the soft band indicate that even in highly obscured AGN a sizeable soft emission can still be produced due to, e.g., scattering, partial covering of the central radiation or from starburst emission around the AGN (e.g. Turner et al. 1997). This confirms that also at these extreme flux levels the ratio between soft and hard X-ray emission is $\sim 1 - 10\%$. In addition, as shown in Barger et al. (2001), the effects of obscuration get significantly reduced at $z \sim 2$, since we observe in the soft band the harder 1.5–6 keV rest frame interval.

When matching the Log N–Log S distribution from ASCA/BeppoSAX with deeper data the presence of a knee is evident. We are able to constrain the Log N–Log S relation below and above the knee, which occurs at $\sim 2 \times 10^{-14}$ erg s $^{-1}$ cm $^{-2}$. We found a fit to the data with a smoothly joined power law with the bright end fixed to the ASCA value (1.67) and the fainter one to $\alpha_{h2} \sim 0.6$. At a level of $\sim 2 \times 10^{-16}$ erg

s $^{-1}$ cm $^{-2}$ we are fully consistent with the UHURU/HEAO-1 estimate, whereas we make up $\sim 68\%$ of the hard XRB, if we assume the BeppoSAX/ASCA value.

A dedicated, multiwavelenght follow up is mandatory to exploit the enormous potential of this (and similar) datasets (Barger et al. 2001; Giacconi et al. 2001b). The identification of X-ray sources at the faintest limit and their optical characterization (by means of photometric redshift) can solve the issue of the evolution of obscured AGN population at very high redshift.

We thank P. Giommi, G. Ghisellini and E. Bertone for useful comments and discussions. We thank the referee for suggestions which improved the paper. We thank the continuous support of the Chandra Help Desk and the CIAO team for the organization of Chandra/CIAO workshop. This work was supported through CNAA, Co-fin and ASI grants.

REFERENCES

Akiyama, M., et al. 2000, ApJ, 532, 700.
 Barger, A.J., Cowie, L.L., Mushotzky, R.F., & Richards, E.A. 2001, AJ, 121, 662.
 Brandt, W.N., et al. 2001, AJ, 122, 1.
 Cagnoni, I., della Ceca, R., & Maccacaro, T. 1998, ApJ, 493, 54.
 Campana, S., Lazzati, D., Panzera, M.R., & Tagliaferri, G. 1999, ApJ, 524, 423.
 Chen, L., Fabian, A.C., & Gendreau, K.C. 1997, MNRAS, 285, 449.
 Chiappetti, L., Cusumano, G., del Sordo, S., Maccarone, M.C., Mineo, T., & Molendi, S. 1998, in *The Active X-ray Sky: Results from BeppoSAX and RXTE*, eds. L. Scarsi, H. Bradt, P. Giommi, & F. Fiore, (Elsevier, Amsterdam), 610.
 della Ceca, R., Braito, V., Cagnoni, I., & Maccacaro, T. 2001, Mem. SAIt, in press (astro-ph/0007430).
 Damiani, F., Maggio, A., Micela, G., & Sciortino, S. 1997, ApJ, 483, 350.
 Fabian, A.C., & Iwasawa, K. 1999, MNRAS, 303, L34.
 Fiore, F., et al. 1999, MNRAS, 306, L55.
 Freeman, D., et al. 2001, ApJ, in press.
 Garmire, G.P., et al. 2001, in preparation.
 Gendreau, K.C., et al. 1995, PASJ, 47, L5.
 Giacconi R., Gursky H., Paolini F. R., & Rossi B. B., 1962, Phys. Rev. Lett., 9, 439.
 Giacconi, R., et al. 2001a, ApJ, 551, 624.
 Giacconi, R., et al. 2001b, to be submitted to ApJS.
 Giommi, P., Perri, M., & Fiore, F. 2000, A&A, 362, 799.
 Grebenev, S. A., Forman, W., Jones, C., & Murray, S.S. 1995, ApJ, 445, 607.
 Harnden, F.R., Jr., et al. 2001, ApJ, 547, L141.
 Hasinger, G., Burg, R., Giacconi, R., Hartner, G., Schmidt, M., Trümper, J., & Zamorani, G. 1993, A&A, 275, 1.
 Hasinger, G., Burg, R., Giacconi, R., Schmidt, M., Trümper, J., & Zamorani, G. 1998, A&A, 329, 482.
 Hasinger, G., et al. 2001, A&A, 365, L45.
 Hornschemeier, A.E., et al. 2000, ApJ, 541, 49.
 Hornschemeier, A.E., et al. 2001, ApJ, 554, 742.
 Ishisaki, Y., et al. 2000, in *Broad Band X-ray Spectra of Cosmic Sources – COSPAR*, eds. K. Makishima, L. Piro, & T. Takahashi (Pergamon Press).
 Lazzati, D., Campana, S., Rosati, P., Chincarini, G., & Giacconi, R. 1998, A&A, 331, 41.
 Lazzati, D., Campana, S., Rosati, P., Panzera, M.R., & Tagliaferri, G. 1999, ApJ, 524, 414.
 Lehmann, I., et al. 2001, A&A, 371, 833.
 Marshall, F.E., et al. 1980, ApJ, 235, 4.
 McCammon, D., Burrows, D.N., Sanders, W.T., & Kraushaar, W.L. 1983, ApJ, 269, 107.
 Moretti, A., Lazzati, D., Campana, S., & Tagliaferri, G. 2001, ApJ submitted.
 Mushotzky, R.F., Cowie, L.L., Barger, A.J., & Arnaud, K.A. 2000, Nat, 404, 459.
 Ogasaka, Y., et al. 1998, *New Horizons from Multi-Wavelength Sky Surveys*, (179th IAU Symposium, Kluwer), eds. B.J. McLean, D.A. Golombek, J.J.E. Hayes, & H.E. Payne, 312.
 Perri, M., & Giommi, P. 2000, A&A, 362, L57.
 Phillips, L.A., Ostriker, J.P., & Cen, R. 2001, ApJ, 554, L9.
 Rosati, P., Burg, R., & Giacconi, R. 1994, in *The Soft X-ray Cosmos* (AIP), eds. E.M. Schlegel & R. Petre, 260.
 Rosati, P., della Ceca, R., Burg, R., Norman, C., & Giacconi, R. 1995, ApJ, 445, L11.
 Rosati, P., et al. 2001, to be submitted to ApJ.
 Schmidt, M., et al. 1998, A&A, 329, 495.
 Schreier, E.J., et al. 2001, ApJ, in press (astro-ph/0105271).
 Setti, G., & Woltjer, L. 1989, A&A, 224, L21.
 Slezak, E., Durret, F., & Gerbal, D. 1994, AJ, 108, 1996.
 Tozzi, P., et al. 2001, ApJ in press (astro-ph/0103014).
 Turner, T.J., George, I.M., Nandra, K., & Mushotzky, R.F. 1997, ApJ, 488, 164.
 Ueda, Y., et al. 1999, ApJ, 518, 656.
 Vecchi, A., Molendi, S., Guainazzi, M., Fiore, F., & Parmar, A.N. 1999, A&A, 349, L73.
 Vikhlinin, A., Forman, W., Jones, C., & Murray, S. 1995, ApJ, 451, 542.
 Vikhlinin, A., et al. 1998, ApJ, 502, 558.
 Weisskopf, M.C., Tananbaum, H.D., Van Speybroeck, L.P., & O'Dell, S.L. 2000, SPIE, 4012, 2.